Journal of Power Sources 195 (2010) 7403–7408

Contents lists available at ScienceDirect

Journal of Power Sources

journal homepage: www.elsevier.com/locate/jpowsour

A three-dimensional macroporous Cu/SnO_2 composite anode sheet prepared via a novel method

Wu Xu*, Nathan L. Canfield, Deyu Wang, Jie Xiao, Zimin Nie, Ji-Guang Zhang

Energy and Environment Directorate, Pacific Northwest National Laboratory, 902 Battelle Boulevard, Richland, WA 99354, USA

ARTICLE INFO

Article history:
Received 19 April 2010
Received in revised form 26 May 2010
Accepted 27 May 2010
Available online 1 June 2010

Keywords:
SnO_2
Composite
Anode material
Porous sheet
Li-ion battery

ABSTRACT

A three-dimensional macroporous Cu/SnO_2 composite anode sheet for lithium ion batteries was prepared via a novel method that is based on selective reduction of metal oxides at appropriate temperatures. SnO_2 particles were imbedded on the Cu particles within the three-dimensionally interconnected Cu substrate, and the whole composite sheet was used directly as an electrode without adding extra conductive carbons and binders. Compared with the SnO_2-based electrode prepared via the conventional tape-casting method on Cu foil, the porous Cu/SnO_2 composite electrode shows significantly improved battery performance. This methodology produces limited wastes and is also adaptable to many other materials. It is a promising approach to make macroporous electrode for Li-ion batteries.

1. Introduction

SnO_2 has been investigated extensively as an alternative anode material to replace graphite in Li-ion batteries during the last decade because it has theoretical specific capacity (782 mAh g^{-1}) as twice as graphite [1–10]. Different nanostructures of SnO_2 have been reported, such as thin films [1], nanowires [2,3], nanoparticle composites (with carbon, polypyrrole, glucose, and others) [4–7], core–shell structure [8], and three-dimensional (3D) structures including porous SnO_2 particles [9] and SnO_2/graphene structure [10]. However, the practical application of SnO_2 has been limited by its poor cycle life and fast capacity fade resulted from the electrode cracking and pulverization which is caused by the huge volume change associated with Li alloying into and de-alloying from the formed Sn.

It has been reported that porous 3D supporting materials are helpful in accommodating the high volume changes of the high-capacity anode materials such as silicon, tin and alloys during the charge/discharge cycles [11,12]. Recently we developed a novel method to prepare macroporous metal substrates as current collectors for Li-ion batteries [13]. Significant improvement in battery performance of Si materials has been achieved. Here we extend this effort to prepare 3D macroporous Cu/SnO_2 composite anode sheets for Li-ion batteries with a modified method, which is based on selective reduction of metal oxides at appropriate temperatures. There are no conductive carbon and binder in the composite anode sheets, and the macroporous structures could accommodate volume expansions from the generation of Li_2O and Li alloying to formed Sn. This method is simple, and it is suitable for producing a large quantity of porous composite anode sheets for battery applications.

2. Experimental

2.1. Preparation of materials

All chemicals used in this work were obtained from commercial sources and used as received. CuO (particle size <5 μm, from Sigma–Aldrich) and SnO_2 (particle size 22–43 nm, from Alfa Aesar) at a weight ratio of 11.3:1 were well mixed with carbon black (from Cancard Ltd., Canada) and poly(vinylbutyral) (from Solutia Inc.) in ethanol–methyl ethyl ketone (1:4 by vol., both from Sigma–Aldrich), where the carbon black acted as a pore-forming agent. The slurry was tape-cast onto a silicone-coated Mylar carrier film, dried in air overnight, and cut into pieces of a desired size. Two pieces of free-standing tapes were laminated under 40 psi and 135 °C, and sintered in air at 1000 °C for 3 h to burn out all carbon black and organic materials to generate a porous structure. Then the sintered sheet was reduced in pure H_2 at 400 °C for 4 h to allow all CuO particles to be reduced to Cu but no SnO_2 to be reduced. When the reduction was completed, the sheet was calcinated in purified argon at 900 °C for 5 h to build up the mechanical strength. After the temperature was cooled to RT under argon, the free-standing porous Cu/SnO_2 composite anode sheet had a thickness of about

* Corresponding author. Tel.: +1 509 375 6934; fax: +1 509 375 3864.
E-mail address: wu.xu@pnl.gov (W. Xu).

0378-7753/$ – see front matter © 2010 Elsevier B.V. All rights reserved.
doi:10.1016/j.jpowsour.2010.05.054

60 μm and a SnO_2 content of 10.0% by weight. The volume loading rate of SnO_2 in this electrode was calculated as 0.547 g cm^{-3}. The mechanical strength was good enough for folding and battery assembly.

As a comparison, a SnO_2 electrode with Super P (SP, from Timcal), and polyvinylidene fluoride (PVDF, from Arkema) was prepared via the conventional tape-casting method by coating the mixture slurry on a 25.4-μm thick Cu foil. The weight ratio of the nano-sized SnO_2, SP and PVDF in the laminate was 8:1:1. The weight percentage of SnO_2 in this electrode (including Cu substrate) was about 9.8% and the volume loading rate of SnO_2 was 0.585 g cm^{-3} electrode, both of which are comparable with SnO_2 in the porous Cu/SnO_2 composite electrode sheet.

2.2. Characterization

The open porosity of the porous Cu/SnO_2 composite sheet was measured using Archimedes' method and calculated using its formula. Average values were obtained by running three samples.

$$\text{Open porosity}(\%) = \frac{\text{Saturated mass} - \text{Dry mass}}{\text{Saturated mass} - \text{Suspended mass}} \times 100\%$$

X-ray diffraction (XRD) was determined on a Philips Xpert X-ray diffractometer with Cu Kα radiation at λ1.54 Å, from 20° to 80° at a scanning rate of 2° min^{-1}. Scanning electron microscopy (SEM) micrographs were collected using a JEOL 5900 scanning electron microscope at a working distance of 12 mm and an accelerating voltage of 20 keV.

The microstructural and microchemical characterization of the porous Cu/SnO_2 composite was performed on a JEOL 5900 scanning electron microscope (SEM) equipped with an EDAX energy dispersive x-ray spectroscopy (EDS) system using Genesis v6.1 software. Imaging and analysis conditions were done at an accelerating voltage of 15 kV. For EDS analysis, the electron beam current was adjusted to obtain approximately 3 kcps with less than 20% dead time using 10-μs amplification time constant. Spectral mapping (e.g. EDS dot maps) was performed to collect EDS spectra on a pixel by pixel basis and to show the spatial distribution of the different elements. Drift corrected EDS dot maps (with a 256 × 200 pixel resolution) were collected in a fast map mode with 300 μs dwell time per pixel, integrating the results from 516 frames. The total number of counts in the sum spectrum was 1.7 million. The regions of interest selected for display were the K-line for oxygen (0.523 keV), and the L-lines for tin (3.443 keV) and copper (0.930 keV), and the results were normalized to 100%. The color intensity in the maps represents the relative concentration of the various elements based on the net intensity of the spectra collected at each pixel.

2.3. Electrochemical performance

Half cells of 2325 type containing the two kinds of SnO_2-electrodes were assembled on a pneumatic coin cell crimper (from Canada National Research Council) at a gas pressure of 200 psi inside an MBraun glovebox filled with purified argon, with Li metal as the counter electrode. A battery-grade electrolyte of 1.0 M $LiPF_6$ in a solvent mixture of ethylene carbonate (EC) and dimethyl carbonate (DMC) at a volume ratio of 1:2 (from Novolyte Technologies) was added, and two pieces of Celgard® 3501 polypropylene microporous membrane was used as the separator. The assembled coin cells were discharged and charged on an Arbin BT-2000 Battery Tester between 0.02 and 2.0 V vs. Li^+/Li at a constant current rate of $C/20$ where the capacity C was based on the theoretical specific capacity of SnO_2. The cyclic voltammograms (CV) of the two SnO_2-electrodes were measured on a CHI 660C Potentiostat/Galvanostat between 3.0 and 0.01 V at a scan rate of 0.1 mV s^{-1} with Li metal as counter and reference electrode.

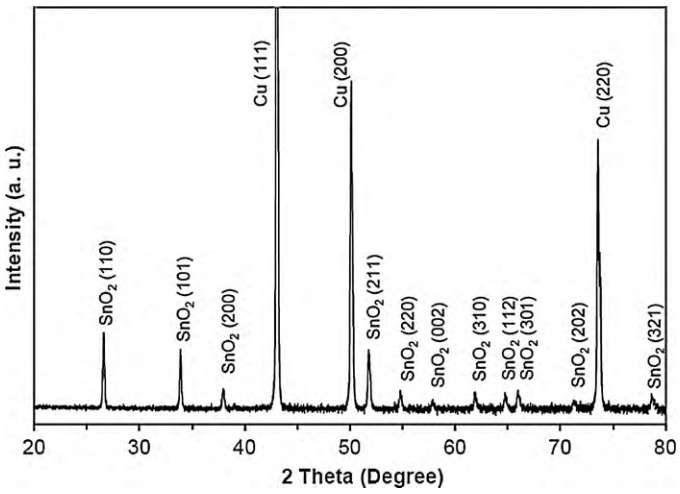

Fig. 1. XRD pattern of the Cu/SnO_2 composite sheet.

3. Results and discussion

Fig. 1 shows the XRD pattern of the porous Cu/SnO_2 composite sheet. The diffraction peaks at 2θ of 43.06°, 50.12° and 73.55° are ascribed to Cu, while all other diffraction peaks are well indexed to a tetragonal SnO_2 with Primitive lattice and $P4_2/mnm$ space group (according to JCPDS #41-1445). No characteristic peaks are found for CuO and Sn, indicating that all CuO particles have been reduced but no SnO_2 particles are reduced during the preparation process.

The morphology and porous structure of the Cu/SnO_2 composite sheet are illustrated by the SEM images in Fig. 2(a and b) in two magnitude scales. The nano-sized particles are well distributed on the micro-sized particles of the porous composite sheet. A macroporous structure is also clearly observed, and the average open porosity of this porous sheet is ca. 46% from the measurement using Archimedes' method.

The EDS dot map images showing the location of each element within the Cu/SnO_2 composite sample are shown in Fig. 3. Fig. 3(a) shows the SEM morphology of the referenced location from which the dot map data were collected. The image in Fig. 3(b) shows an overlay of the Cu (L-line) and Sn (L-line) net intensities for the dot map. It is clearly seen that the Sn (in pink color) resides only in the areas of the small particles that decorate the surface of the sample, and the Cu (in green color) is detected only in the large particles of the sample. Similarly, it is noticed from the image in Fig. 3(c) showing an overlay of Cu (L-line) and O (K-line) net intensities for this dot map that the Cu (in green color) is detected only in the large particles of the sample and the O (in red color) is only detected in the small particles that decorate the surface of the sample.

When the net intensities of Cu, Sn and O are overlaid in one image (Fig. 3d), it can be seen that the red is intermixed and well overlapped with the pink in the small surface particles, yet no red is detected in any of the green regions where the large particles are located. It means that both Sn (pink) and O (red) are only detected in the small particles decorating the surface, while only Cu (green) is detected in the large particles. It should be noted that the signal from the O is substantially lower than those from the Cu and Sn, and therefore in the composite shown in Fig. 3d, the O is somewhat swamped out by the Sn. However, Fig. 3c clearly shows that there is O in all of the small surface particles shown in the image, thus reinforcing the conclusion that the Sn exists as an oxide while the Cu is in pure metal. With the combination of the XRD data in Fig. 1, it is therefore proved that the small particles are SnO_2 and the large particles are pure metal Cu without any CuO.

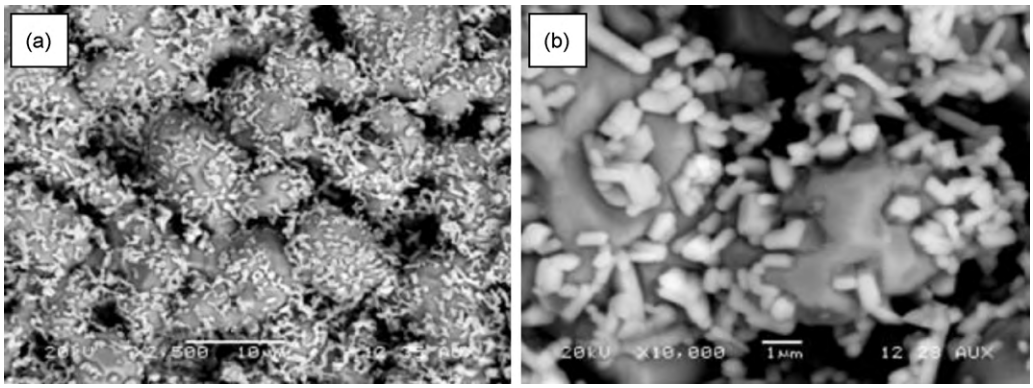

Fig. 2. SEM surface images of the porous Cu/SnO_2 composite sheet in two magnitude scales.

Fig. 4 compares the CV curves of the macroporous Cu/SnO_2 composite sheet (a) with the SnO_2/SP/PVDF electrode coated on Cu foil (b). The CV curves during the first scan are different from the subsequent scans for both samples. The sharp, irreversible peak at about 0.7 V (peak A) on the first cathodic scan is attributed to the reduction of SnO_2 to metallic Sn, and the broad reduction peak from ca. 0.6 to 0.01 V (labeled B and C) is related to the alloying of Li into Sn to form Li_xSn ($0 \le x \le 4.4$). The electrode is activated after the first cathodic scan to 0.01 V vs. Li.

As for the porous Cu/SnO_2 composite anode in Fig. 4(a), the Li de-alloying from Li_xSn is reversible during the subsequent anodic scan. It is noticed that two broad oxidation peaks A'_2 and A'_1 appear at about 1.3 and 1.9 V, respectively. These two oxidation peaks (A'_1 and A'_2) are paired with the reduction peaks marked as A_1 (1.3 V) and A_2 (0.9–1.0 V) which are derived from peak A to form two redox couples. The two redox couples (A_1/A'_1 and A_2/A'_2) are most likely ascribed to the partially reversible reactions ((1) and (2) below) to some extent, respectively, as reported in previous literature [14,15]. The good reversibility of the two redox reactions is mainly due to the good electrical contact of SnO_2 particles on Cu substrate, where the SnO_2 particles are imbedded among the Cu particles during this unique preparation process.

$$SnO_2 + 2Li^+ + 2e^- \rightarrow SnO + Li_2O \quad (1)$$

$$SnO + 2Li^+ + 2e^- \rightarrow Sn + Li_2O \quad (2)$$

The peak B is also split into two separate peaks (B_1 and B_2) after the first cathodic scan. The Li alloying and de-alloying process in the porous Cu/SnO_2 composite anode shows three pairs of reversible redox peaks: B_1/B'_1, B_2/B'_2 and C/C'.

As for the SnO_2/SP/PVDF electrode in Fig. 4(b), it also shows similar oxidation peaks (A'_2 and A'_1) and the partially reversible redox

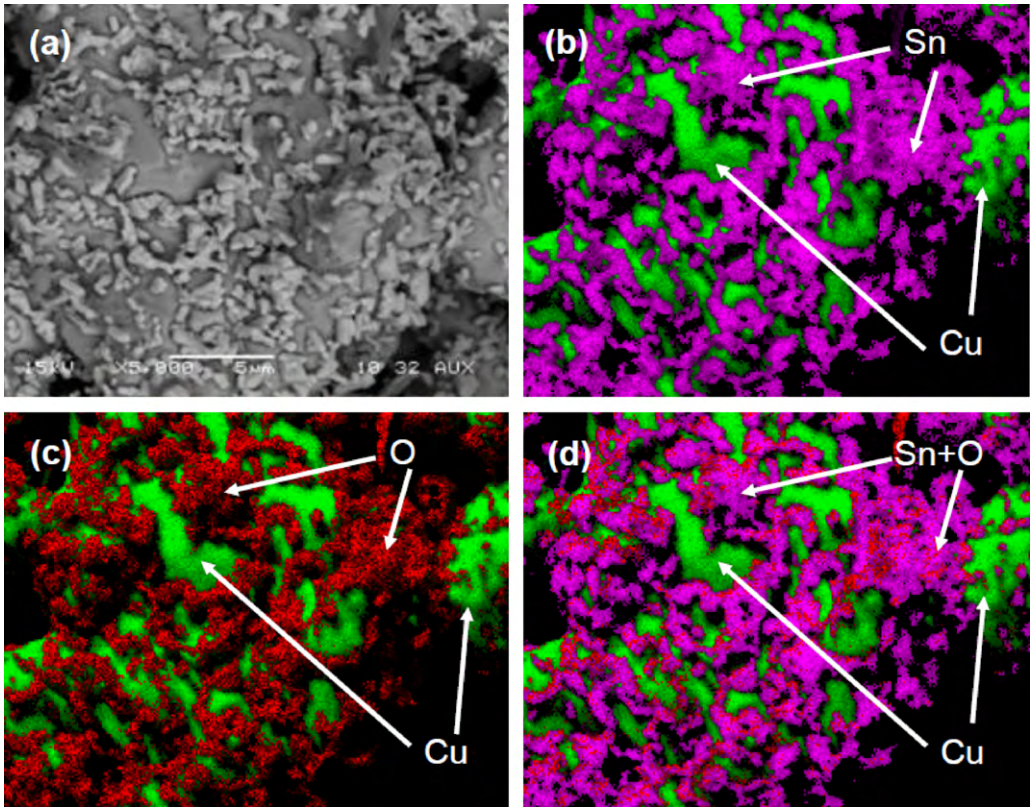

Fig. 3. Microstructural and microchemical images of the porous Cu/SnO_2 composite sheet: (a) surface SEM of the location where the EDS dot map data were collected, (b) EDS dot map with overlays of Cu (green) and Sn (pink), (c) EDS dot map with overlays of Cu (green) and O (red), and (d) EDS dot map with overlays of Cu (green), Sn (pink) and O (red). (For interpretation of the references to color in Fig. 3, the reader is referred to the web version of the article.)

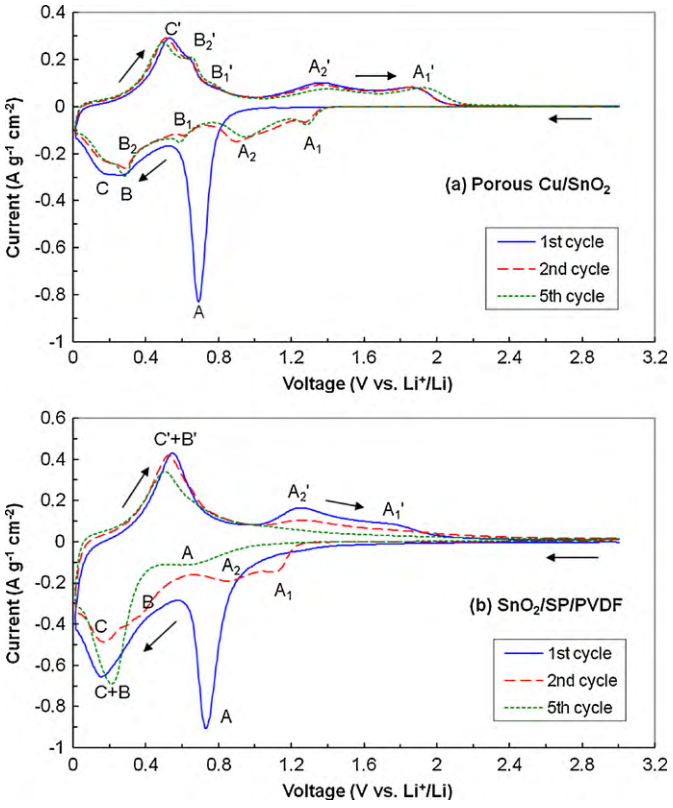

Fig. 4. Cyclic voltammographs of porous Cu/SnO_2 composite electrode compared with SnO_2/SP/PVDF electrode, in the voltage range of 0.01–3.0 V at a scan rate of 0.1 mV s^{-1}.

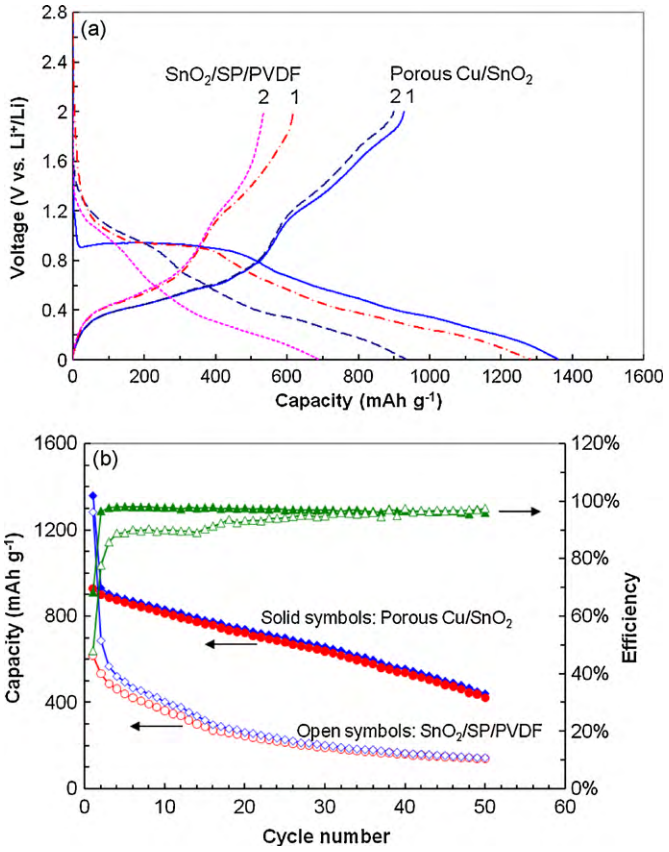

Fig. 5. Charge–discharge profile and cycling performance of porous Cu/SnO_2 composite compared with SnO_2/SP/PVDF electrode. Symbols in (b): diamonds for Li-insertion capacity, circles for Li de-insertion capacity, and triangles for coulombic efficiency.

reactions related to SnO/Sn (A_2'/A_2) and SnO_2/SnO (A_1'/A_1), like the porous Cu/SnO_2 composite anode does. However, these reactions diminish quickly thus no corresponding redox peaks are observed in the fifth scan. The Li alloying/de-alloying process does not show well-defined redox peaks except for one major redox peaks at ca. 0.2/0.5 V mainly because of the poor electrical contact among Sn/Li_2O with conductive carbon (SP) and Cu substrate after several cycles of huge volume change.

Fig. 5(a) shows the discharge–charge curves of the porous Cu/SnO_2 composite electrode and the SnO_2/SP/PVDF on Cu foil in half cells during Li alloying and de-alloying processes. The plateaus on the charge or discharge curves are related to the redox reactions on the CV curves during cathodic or anodic scans shown in Fig. 4(a) and 4(b). The Li-insertion/de-insertion capacity for SnO_2 during the first discharge/charge cycle is 1358/928 mAh g^{-1} for the porous Cu/SnO_2 composite and 1282/617 mAh g^{-1} for the SnO_2/SP/PVDF on Cu foil. The corresponding capacity loss is 430 and 665 mAh g^{-1}, and the coulombic efficiency of the first cycle is 68.3 and 48.1%, respectively. The irreversible capacity loss is mainly from two parts—decomposition of electrolyte and loss of electrical contact. The electrolyte decomposition during the 1st cycle is to form the solid electrolyte interface (SEI) layer on the electrode surface and is mostly related to the electrode surface area. Higher surface area leads to more electrolyte decomposition thus higher irreversible capacity loss. The porous Cu/SnO_2 composite has higher surface area than the electrode of SnO_2/SP/PVDF on Cu foil so the porous Cu/SnO_2 composite has higher capacity loss from electrolyte decomposition than the latter.

The second portion of the irreversible capacity loss is due to the loss of electrical contact among active material particles with conductive particles and substrate. After the reduction of SnO_2 to metallic Sn and Li-insertion into Sn to form Li_xSn, the huge volume expansion leads to the deformation of the electrode and large stress is built up if the electrode deformation is restricted. Then, during the Li de-alloying process, the good electrical contact among the active material particles and conductive particles and/or substrate may be lost in some areas due to the volume extraction. Thus some Li in the formed Li_xSn cannot be de-alloyed, and a capacity loss appears. In the porous Cu/SnO_2 composite electrode, the volume expansion can be well accommodated and the stress among the particles can be easily released by the porous structure. The good electrical contact of the particles is still maintained during Li de-alloying so the capacity loss due to electrical contact loss is limited in the porous Cu/SnO_2 composite electrode, then the total capacity loss for this electrode is mainly from electrolyte decomposition. However, the electrode of SnO_2/SP/PVDF on Cu foil cannot avoid such kind of electrical contact loss, and it shows extra capacity loss besides from electrolyte decomposition. Therefore, it shows larger total capacity loss and lower coulombic efficiency than the porous Cu/SnO_2 composite.

It is also seen from Fig. 5(a) that the porous Cu/SnO_2 composite electrode shows larger SnO_2 reduction region at ca. 0.9 V (0–500 mAh g^{-1}) than the coated SnO_2/SP/PVDF electrode (200–400 mAh g^{-1}) in the first Li-insertion (i.e. discharge of the Li/SnO_2 half cell) process. It is most likely attributed to the higher conductivity and more particle exposure to electrolyte in the porous Cu/SnO_2 composite electrode. When compared the SEM images (a) and (c) in Fig. 6, there are more SnO_2 exposed to the electrolyte in batteries for the porous Cu/SnO_2 composite electrode than for the SnO_2/SP/PVDF electrode. Thus more SnO_2 can be easily reduced and then alloyed with Li in the porous Cu/SnO_2 composite. On the other hand, SnO_2 in the coated SnO_2/SP/PVDF electrode cannot be completely reduced in the first cycle, and it takes several

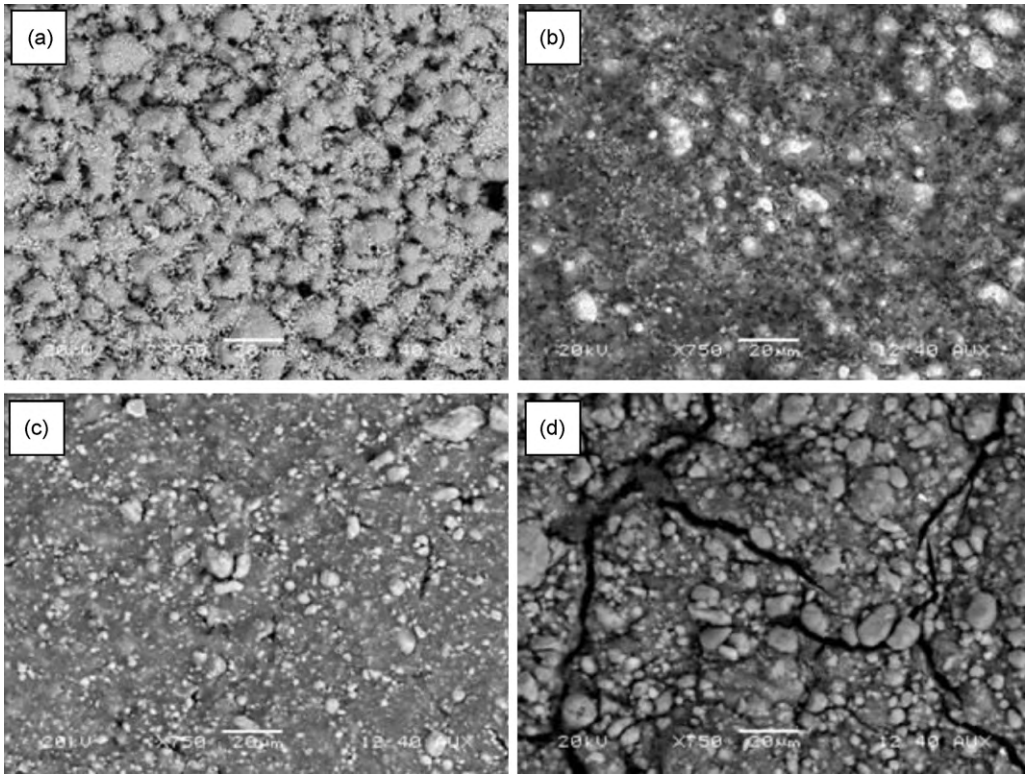

Fig. 6. Comparison of SEM surface images of the two SnO_2-electrodes before and after battery test. Porous Cu/SnO_2 composite electrode before (a) and after (b); SnO_2/SP/PVDF electrode before (c) and after (d).

cycles to be totally reduced, which is also in agreement with the coulombic efficiency increase with cycling shown in Fig. 5(b).

During the first Li-insertion process shown in Fig. 5(a), the porous Cu/SnO_2 composite electrode shows a sharp IR drop when compared to the coated SnO_2/SP/PVDF electrode because it has higher conductivity for the transportation of both lithium ions and electrons. Then the capacity from the IR contribution is small. After the first cycle, the porous Cu/SnO_2 composite electrode has lower conductivity than before because the formed Li_2O particles would slow down the transportation of ions. Then the capacity from the IR contribution increases in the second Li-insertion process. In addition, in the second Li-insertion process, the sample demonstrates a Li-insertion curve of pure Sn, which typically starts at ~1.2 V with a slope. In this regarding, both porous Cu/SnO_2 composite electrode and coated SnO_2/SP/PVDF electrode show similar profile in the second Li-insertion process.

Fig. 5(b) exhibits the battery charge/discharge cycling performance of both SnO_2-electrodes. Obviously, the capacity (for both charge and discharge), coulombic efficiency, and cycle life of the porous Cu/SnO_2 composite electrode are much higher or better than the coated SnO_2/SP/PVDF electrode. As discussed above, this is because the pores in the porous Cu/SnO_2 composite electrode can accommodate the big volume change of Sn particles after Li alloying, the stress among the formed Li_xSn particles can almost be released, and the good electrical contact between the Sn particles and the Cu substrate is maintained even if there is a huge volume change during Li alloying and de-alloying. It is proved from the SEM images of the porous Cu/SnO_2 composite electrode before and after cycling test shown in Fig. 6(a) and (b). Therefore, an excellent battery performance is achieved for the porous Cu/SnO_2 composite electrode. However, the coated SnO_2/SP/PVDF electrode via conventional method cannot compensate the big volume change along the electrode sheet direction and a lot of stress among the particles is generated after Li alloying. Therefore with cycling continuation, cracking occurs on the SnO_2/SP/PVDF laminate and the electrical contact among the active material (Sn particles) and conductive carbon or current collector will be lost in some locations. As seen from Fig. 6(c) and (d) that show the coated SnO_2/SP/PVDF electrode before and after cycling test, some small cracks already exist in the electrode before battery test, and more and larger cracks appear in the coated electrode after cycling. The worst case is the delaminating of SnO_2/SP/PVDF from the Cu current collector. Then the capacity fades quickly and the cycle life is poor.

With the optimization of SnO_2 content, particle size, pore size, pore volume, and other preparation conditions, the porous Cu/SnO_2 composite anode sheets are expected to have even better capacity and cycle life. The results will be reported separately.

4. Conclusions

A new approach is described to produce macroporous Cu/SnO_2 composite anode sheets for lithium ion batteries. This approach is based on selective reduction of metal oxides at appropriate temperatures. SnO_2 particles are imbedded on the as-reduced Cu substrate which works as the current collector and conductive additive. Therefore neither binder nor additional carbon is necessary for this porous Cu/SnO_2 composite anode. The results indicate that the macroporous Cu/SnO_2 composite anode sheets have significantly improved capacity, coulombic efficiency and cycle life compared to the SnO_2 with same particle sizes on Cu foil prepared via the conventional tape-casting method. This methodology is adjustable and can be used in many different areas to fully utilize the current collector and provide good electrical contact between the active material and substrate.

Acknowledgements

This work was sponsored by the Laboratory Directed Research and Development Project of Pacific Northwest National laboratory (PNNL) and the Office of Vehicle Technologies of the U.S. Department of Energy. The authors thank Dr. Bradley R. Johnson and Mr. Jarrod V. Crum of PNNL for helping the dot map test.

References

[1] S.H. Choi, J.S. Kim, Y.S. Yoon, Electrochim. Acta 50 (2004) 547.
[2] Z. Ying, Q. Wan, H. Cao, Z.T. Song, S.L. Feng, Appl. Phys. Lett. 87 (2005) 113108.
[3] M.-S. Park, G.-X. Wang, Y.-M. Kang, D. Wexler, S.-X. Dou, H.-K. Liu, Angew. Chem. Int. Ed. 46 (2007) 750.
[4] L. Yuan, J. Wang, S.Y. Chew, J. Chen, Z.P. Guo, L. Zhao, K. Konstantinov, H.K. Liu, J. Power Sources 174 (2007) 1183.
[5] J. Yao, X. Shen, B. Wang, H. Liu, G. Wang, Electrochem. Commun. 11 (2009) 1849.
[6] Y. Kim, Y. Yoon, D. Shin, J. Anal. Appl. Pyrolysis 85 (2009) 557.
[7] F.M. Courtela, E.A. Baranovab, Y. Abu-Lebdeha, I.J. Davidson, J. Power Sources 195 (2010) 2355.
[8] D. Deng, J.Y. Lee, Chem. Mater. 20 (2008) 1841.
[9] S.-M. Paek, E.J. Yoo, I. Honma, Nano Lett. 9 (2009) 72.
[10] R. Yang, Y. Gu, Y. Li, J. Zheng, X. Li, Acta Mater. 58 (2010) 866.
[11] Y.-L. Kim, Y.-K. Sun, S.-M. Lee, Electrochim. Acta 53 (2008) 4500.
[12] L. Trahey, J.T. Vaughey, H.H. Kung, M.M. Thackeray, J. Electrochem. Soc. 156 (2009) A385.
[13] W. Xu, N.L. Canfield, D. Wang, J. Xiao, Z. Nie, X.S. Li, W.D. Bennett, C.C. Bonham, J.-G. Zhang, J. Electrochem. Soc. 157 (2010) A765.
[14] M. Mohamedi, S.-J. Lee, D. Takahashi, M. Nishizawa, T. Itoh, I. Uchida, Electrochim. Acta 46 (2001) 1161.
[15] T. Brousse, R. Retoux, U. Heerterich, D.M. Schleich, J. Electrochem. Soc. 145 (1998) 1.